doi:10.1017/S1431927614006874
Microsc. Microanal. 20 (Suppl 3), 2014


# Using Bethe Potentials in the Scattering Matrix for Defect Image Simulations

A. Wang[1] and M. De Graef[1]

[1.] Dept. of Materials Science and Engineering, Carnegie Mellon Univ., Pittsburgh PA 15213, USA

Bethe potentials were introduced by Bethe in 1928 to reduce the size of the dynamical matrix in electron scattering problems using first order perturbation theory [1]. The standard approach is to start from the dynamical equations in the Bloch wave representation, and split the set of diffracted beams into two subsets, namely *strong* and *weak* beams, according to some appropriate criterion. While there is some early work on the application of the perturbation approach to the formulation of the dynamical scattering problem via the scattering matrix formalism [2], Bethe potentials have not been used extensively for simulation approaches other than the Bloch wave approach. For defect image contrast simulations, the Bloch wave approach is somewhat tedious, and, traditionally, one has resorted to solving the dynamical equations in differential form, while replacing the standard excitation error by a position dependent, effective excitation error. This works well for defects with continuous displacement fields, such as dislocations and semi-coherent inclusions, but for planar defects, with a discontinuous displacement field, one must include their effect as a separate phase shift of the potential Fourier coefficients. A more coherent approach would be to describe *all* defect displacements in terms of phase shifted Fourier coefficients. In this contribution, we show that by using Bethe potentials in combination with the scattering matrix, one can reduce the size of the dynamical matrix and hence the computation time required for defect image simulations.

For a defect free foil, the dynamical scattering equations can be formulated as follows:

$$\frac{\mathrm{d}\mathbf{S}(z)}{\mathrm{d}z} = \mathrm{i}\mathcal{A}(\mathbf{r})\mathbf{S}(z),$$

where $\mathcal{A}$ is the *structure matrix*, which has $2\pi s_g + \pi/q_0$ along its diagonal, and $\pi/q_{g-g'}$ for the off-diagonal entries; $s_g$ is the excitation error, and the factors $1/q_g$ are proportional to the Fourier coefficients of the optical potential. The scattered amplitudes are represented as a column vector S($z$). In the presence of defects, the off-diagonal matrix elements are multiplied by the phase factor $\exp[-\mathrm{i}\alpha_{g-g'}(\mathrm{r})]$, where $\alpha_g(\mathrm{r}) = 27\pi\mathrm{g}\cdot\mathbf{R}(\mathrm{r})$ and $\mathbf{R}(\mathrm{r})$ is the combined displacement field of all lattice defects. Reducing the number of entries in the structure matrix $\mathcal{A}$ leads to a smaller scattering matrix $\mathcal{S}(z) \equiv \exp[\mathrm{i}\mathcal{A}z]$ and, hence, a shorter simulation time. As illustrated in Fig. 1 in ref. [2], some beams contribute only weakly to the images; therefore, these beams can be incorporated into the strong beams by means of the Bethe potential perturbation approach. When applied to the structure matrix in the dynamical scattering equation above, one obtains modified matrix elements for the strong beams of the form:

$$\bar{\mathcal{A}}_{nn'} = \mathcal{A}_{nn'} - \sum_{l=k+1}^{N} \frac{\mathcal{A}_{nl}\mathcal{A}_{ln'}}{\mathcal{A}_{ll} - \mathcal{A}_{n'n'}};$$

the sum over $l$ covers only the weak beams. The criterion for a beam to be considered weak is: $|s_{\mathbf{g}}| \ll \lambda|U_{g-h}|$, where $\lambda$ is the wavelength and $|U_{g-h}|$ is the Fourier coefficient between beams g and h. Our simulations show that a beam g should be considered to be strong when $|s_{\mathbf{g}}|/\lambda|U_{g-h}| \leq 20$ while a beam g for which $20 < |s_{\mathbf{g}}|/\lambda|U_{g-h}| \leq 40$ would be considered weak; note that this condition must be satisfied for all beams h. All beams g for which $40 < |s_{\mathbf{g}}|/\lambda|U_{g-h}|$ for all h can be ignored.

As an illustration of this perturbation approach, we show a 200 kV systematic row simulation for a defect free Cu foil in Figure 1. The solid curves show the intensity as a function of thickness using the full 17-beam (–8g, –7g. . . , 7g, 8g) calculation, with g = (111). The red dots show the intensity using 8 strong beams (–3g, –2g. . . , 3g, 4g) and 4 Bethe-approximated weak beams (-5**g**, -4**g**, **5g** and 6**g**), selected according to the above criterion. A similar simulation for a spherical inclusion with radius of 20 nm located at the center of a 256 × 256 × 256 nm foil is shown in Figure 2. The inclusion has a lattice misfit of about 5% which places the surrounding matrix in compression. The beam selection is the same as for Figure 1. From these examples, it is clear that simulations using a reduced scattering matrix $\mathcal{S}(z)$, incorporating weak beams by means of Bethe potentials, produce results that are virtually identical to those using a full size dynamical matrix, but the computation time using the reduced scattering matrix is decreased by about 40%. The combination of Bethe potentials and the scattering matrix can also be applied to other many-beam defect contrast simulations, such as annular dark field STEM diffraction contrast images and electron channeling contrast images in the SEM.

References:

[1] H.A. Bethe. Ann. d. Physik **87** (1928), p.55.
[2] J.M. Zuo and A.L. Wieckenmeier, Ultramicroscopy **57** (1995), p.375
[3] Research supported the Air Force Office of Scientific Research, MURI contract # FA9550-12-1-0458.

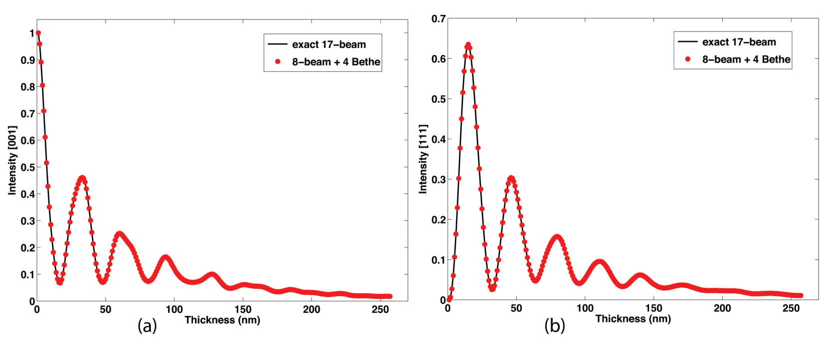


**Figure 1.** Comparison of the intensities of systematic row simulations using 17 beams (solid lines) and 8-beam calculations with 4 weak beams for (a) the center beam (000) and (b) the (111) reflection in a defect free Cu foil at 200 ke V.

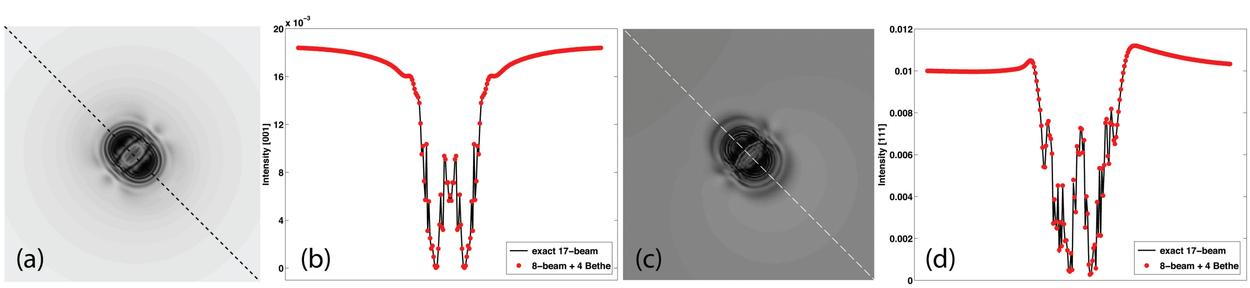


**Figure 2.** Comparison of the intensities of systematic row simulations for a spherical inclusion in a cubic 256 nm Cu foil using 17 beams and an 8-beam calculation with 4 weak beams. (a) Bright-field imaging and (b) line profiles obtained along dashed line in (a); (c) dark-field (111) imaging and (d) the diagonal line profiles.

https://doi.org/10.1017/S1431927614006874 Published online by Cambridge University Press